Short rticle

Cell Stem Cell

# Notch-Induced miR-708 Antagonizes Satellite Cell Migration and Maintains Quiescence

## Graphical Abstract

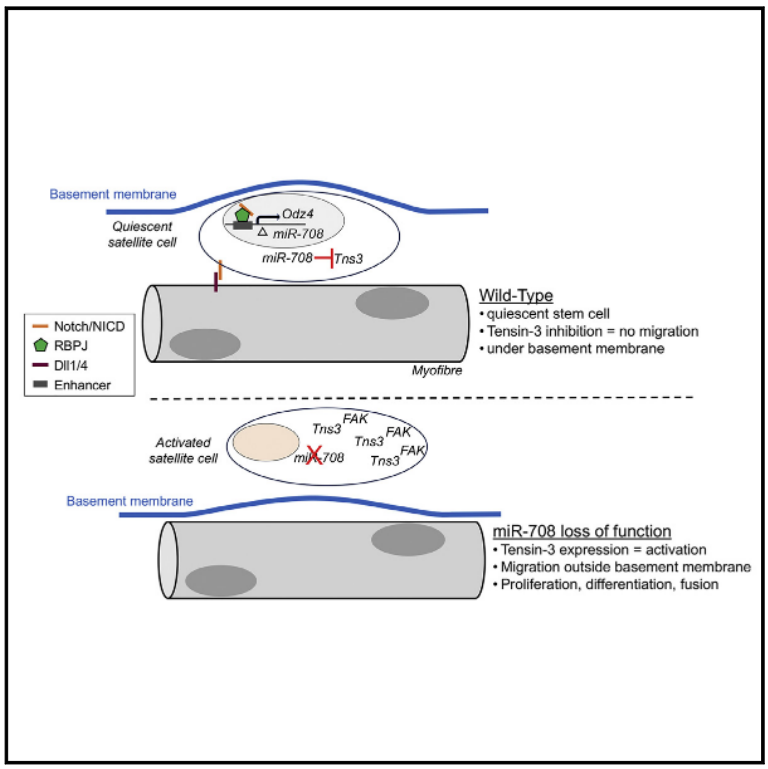


## Highlights

Notch induces the transcription of microRNA-708, a quiescence-specific mirtron

*In vivo* inhibition of miR-708 disrupts satellite cell quiescence and self-renewal

miR-708 antagonizes Tensin3 to inhibit FAK activation

Active repression of migration stabilizes quiescent stem cells in their niche

## Authors

Meryem B. Baghdadi, Joao Firmino, Kartik Soni, ..., Philippos Mourikis, David Castel, Shahragim Tajbakhsh

## Correspondence

shahragim.tajbakhsh@pasteur.fr

## In Brief

Baghdadi et al. show that Notch signaling induces transcription of the quiescence-specific mirtron miR-708 that represses Tensin3, a component of the focal adhesion complex. This repression inhibits FAK activation, which in turn stabilizes satellite cells within their niche. miR-708 regulates quiescence and self-renewal by active repression of cell migration.

Baghdadi et al., 2018, Cell Stem Cell *3*, 859–868
December 6, 2018 
https://doi.org/10.1016/j.stem.2018.09.017

CellPress

Cell Stem Cell
Short Article

# Notch-Induced miR-708 Antagonizes Satellite Cell Migration and Maintains Quiescence

Meryem B. Baghdadi,[1,2,3] Joao Firmino,[4] Kartik Soni,[1,2] Brendan Evano,[1,2] Daniela Di Girolamo,[1,5] Philippos Mourikis,[6] David Castel,[7,8] and Shahragim Tajbakhsh[1,2,9,*]
[1]Stem Cells and Development, Department of Developmental & Stem Cell Biology, Institut Pasteur, Paris 75015, France
[2]CNRS UMR 3738, Institut Pasteur, Paris 75015, France
[3]Sorbonne Universités, UPMC, University of Paris 06, IFD-ED 515, Paris 75252, France
[4]Bioimaging and Optics platform (BIOP), School of Life Sciences, Swiss Federal Institute of Technology (EPFL), Lausanne, Switzerland
[5]Dipartimento di Medicina Clinica e Chirurgica, Università degli Studi di Napoli Frederico II, 80131 Naples, Italy
[6]INSERM IMRB U955-E10, UPEC, ENVA, EFS, Créteil 94000, France
[7]UMR8203 "Vectorologie et Thérapeutiques Anticancéreuses," CNRS, Gustave Roussy, Université Paris-Sud, Université Paris-Saclay, 94805 Villejuif, France
[8]Département de Cancérologie de l'Enfant et de l'Adolescent, Gustave Roussy, Université Paris-Sud, Université Paris-Saclay, 94805 Villejuif, France
[9]Lead Contact
*Correspondence: shahragim.tajbakhsh@pasteur.fr
https://doi.org/10.1016/j.stem.2018.09.017

## SUMMARY

**Critical features of stem cells include anchoring within a niche and activation upon injury. Notch signaling maintains skeletal muscle satellite stem) cell quiescence by inhibiting differentiation and inducing expression of extracellular components of the niche. However, the complete spectrum of how Notch safeguards quiescence is not well understood. Here, we perform Notch ChIP-sequencing and small RNA sequencing in satellite cells and identify the Notch-induced microRNA-708, which is a mirtron that is highly expressed in quiescent cells and sharply downregulated in activated cells. We employ *in vivo* and *ex vivo* functional studies, in addition to live imaging, to show that miR-708 regulates quiescence and self-renewal by antagonizing cell migration through targeting the transcripts of the focal-adhesion-associated protein Tensin3. Therefore, this study identifies a Notch-miR708-Tensin3 axis and suggests that Notch signaling can regulate satellite cell quiescence and transition to the activation state through dynamic regulation of the migratory machinery.**

## INTRODUCTION

The regenerative ability and plasticity of adult skeletal muscle is largely due to its resident muscle satellite cells (Sambasivan and Tajbakhsh, 2015). In resting muscle, satellite cells are quiescent and express the paired-box transcriptional factor *Pax7* (Seale et al., 2000). Following injury, they re-enter the cell cycle and proliferate to generate myoblasts that further differentiate and fuse to restore the damaged fiber, while a subpopulation of myogenic cells returns to quiescence for self-renewal of the satellite cell pool (Baghdadi and Tajbakhsh, 2018).

Notch is a crucial regulator of satellite cells as the satellite cell-specific depletion of RBPJ, the DNA binding factor essential for mediating canonical Notch signaling, leads to spontaneous differentiation and progressive loss of satellite cells (Mourikis et al., 2012b; Bjornson et al., 2012). Notch activity antagonizes myogenesis by induction of transcriptional repressors (members of the HES and/or HEY family) (Mourikis et al., 2012b; Bjornson et al., 2012), and we recently showed that Notch-induced production of Collagen V by satellite cells is a critical component of the quiescent niche, as its depletion leads to gradual diminution of the stem cell pool (Baghdadi et al., 2018). However, it remains unclear whether this pleiotropic signaling pathway maintains stem cells by controlling additional cellular processes other than differentiation and niche composition.

MicroRNAs (miRNAs) are essential for muscle homeostasis and regeneration upon injury as the conditional deletion of *Dicer* (an RNase III endonuclease required for maturation of miRNAs) in the $PAX7^{+}$ population, results in a depletion of satellite cells and a quasi-absence of repair upon injury (Cheung et al., 2012). Although numerous miRNAs were reported to regulate myoblast proliferation and differentiation (Kirby et al., 2015), only miR-489 (Cheung et al., 2012) was shown to regulate satellite cell quiescence and/or self-renewal.

We performed RNA sequencing on primary skeletal muscle cells (Castel et al., 2018) and identified the quiescence specific miR-708 that is regulated by Notch signaling. We show that this micro-RNA plays a critical role in satellite cell maintenance and migration in the niche by targeting *Tensin3* (*Tns3*) mRNA, which encodes a fibrillar adhesion protein that physically links integrins and the actin cytoskeleton (Qian et al., 2009). Therefore, we identify a miR-708 that acts as a gatekeeper of quiescence by modulating muscle stem cell migration.

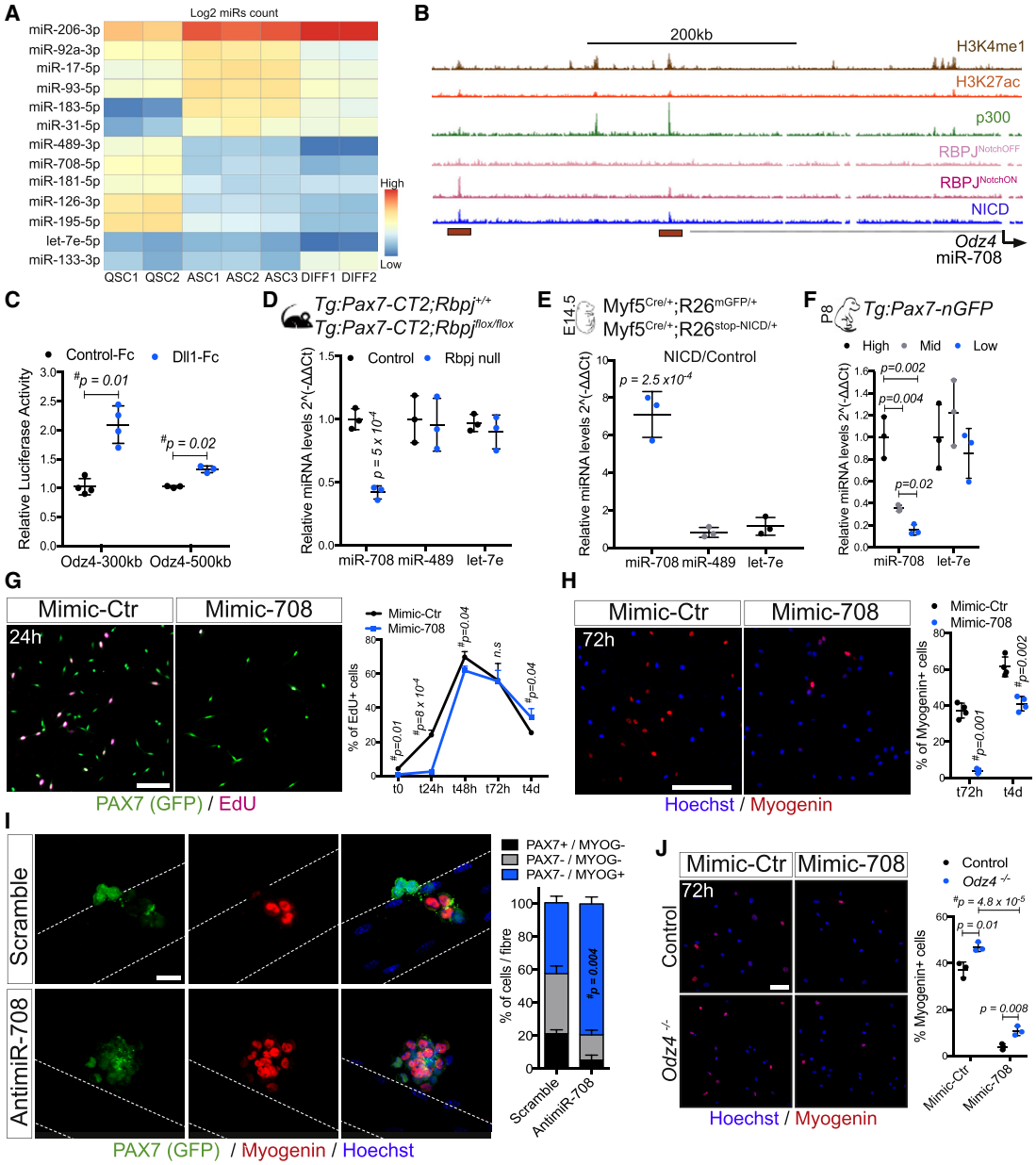


**Figure 1. miR-708 a Notch Pathway Target Mirtron Specifically Expressed in Quiescent Satellite Cells Suppresses Proliferation and Differentiation while Its Inhibition Impairs Self-Renewal**

(A) Gene expression from RNA deep sequencing of freshly isolated satellite cells from *Tg:Pax7-nGFP* adult mice (QSC, n = 2), *in vitro*-activated satellite cells for 60 hr (ASC, n = 3), and differentiated cells cultured for 7 days (DIFF, n = 2).

(B) ChIP-seq tracks showing NICD and RBPJ occupancy on enhancers associated with mouse *Odz4* locus. Orange rectangle indicates RBPJ binding positions.

(C) Transcriptional response measured by Firefly luciferase signal of two enhancers of *Odz4* to activation of Notch signaling in C2C12 cells cultured on Dll1-Fc. Control Fc is set at 1; n = 3 independent assays.

(D) Real-time qPCR analysis of miR-708 in Control (*Tg:Pax7-CT2; Rbpj*$^{+/+}$) and *Rbpj* conditional KO (*Rbpj* null; *Tg:Pax7-CT2; Rbpj*$^{flox/flox}$) satellite cells isolated from resting muscles.

(E) Induction of miR-708 in E14.5 control (*Myf5*$^{Cre/+}$*; R26*$^{mTmG/+}$) and *Myf5*$^{Cre}$*-NICD* (*Myf5*$^{Cre/+}$*; R26*$^{stop\text{-}NICD\text{-}nGFP/+}$) myogenic cells isolated by FACS, assessed by real-time qPCR. Results are presented as a ratio of expression in NICD over Control. let-7e is not a Notch target; n = 4 mice or fetuses per genotype.

(F) Transcript expression levels of miR-708 targeted by Notch in cells fractionated by FACS based on GFP intensity from *Tg:Pax7-nGFP* mice at postnatal day 8 (P8): Pax7$^{High}$ (20%), Pax7$^{Mid}$ (40%), and Pax7$^{Low}$ (20%); n = 3 pups.

(G) EdU reaction and GFP staining of satellite cells isolated from *Tg:Pax7-nGFP* mice 24 hr after Mimic-708 or Control (Ctr) transfection. Time course of proliferation by quantification of EdU 24 hr to 4 days following miR-708 overexpression (Mimic-708) or Control is shown.

(H) Myogenin staining of satellite cells isolated from *Tg:Pax7-nGFP* mouse 72 hr after Mimic-708 or control Scramble transfection. Quantification of Myogenin$^{+}$ cells at 72 hr and 4 days following treatment; n = 4 mice, ≥400 cells, 2 wells/condition is shown.

*legend continued on next page)*

## RESULTS

### A Quiescence-Specific miRNA Is Regulated by Notch Signaling in Satellite Cells

To identify miRNAs that regulate cellular quiescence, we performed RNA deep sequencing on freshly isolated satellite cells (QSC), *in vitro*-activated satellite cells for 60 hr (ASC) and differentiated cells cultured for 7 days (DIFF) (Figure 1A; (Castel et al., 2018)). We found that miR-708 was enriched in quiescent satellite cells (Figure 1A). Real-time qPCR analysis showed miR-708 expression to be significantly decreased *in vivo* in ASCs 5 days post-injury, and in freshly isolated myofibers compared to freshly isolated satellite cells (Figure S1A). Interestingly, miR-708 is a highly conserved mirtron (Ruby et al., 2007) encoded in the quiescence-specific gene *Odz4*/*Tenm4* (Figure S1B). As is the case with other mirtrons, miR-708 does not have its own promoter; therefore, its expression depends on that of *Odz4*.

Interestingly, *Odz4* expression decreases in Notch-depleted myogenic progenitors in embryos (*Pax3*$^{Cre/+}$*; Rbpj*$^{-/-}$*; Myod*$^{-/-}$) (Bröhl et al., 2012) suggesting a potential link with Notch signaling. We confirmed this hypothesis by interrogating genome-wide chromatin immunoprecipitation sequencing (ChIP-seq) data in adult murine myoblasts (Castel et al., 2013). Notably, two NICD and RBPJ binding sites were identified as most proximal to the *Odz4* locus (Figure 1B). The combination of histone modifications H3K4me1, H3K27ac, and the acetyltransferase p300 (Figure 1B), in addition to their ability to induce transcription upon Notch activation in cell-based luciferase assays (Figure 1C), indicates that these sequences are in bona fide enhancers.

Using genetically modified mice for Notch ablation (*Tg:Pax7-CT2; Rbpj*$^{flox}$ [Mourikis et al., 2012b]; Figures 1D and S1C) or gain-of-function (*Myf5*$^{Cre}$*;R26*$^{NICD\text{-}nGFP}$ [Mourikis et al., 2012a], Figures 1E and S1D), we showed that transcription of miR-708 (but not miR-489, another quiescent miRNA [Cheung et al., 2012]) and *Odz4* tightly followed Notch activity. We confirmed their transcriptional responses in satellite cells isolated from *Tg:Pax7-nGFP* postnatal day 8 (P8) pups in which endogenous Notch activity gradually declines as cells transit from an upstream Pax7$^{High}$ to a committed Pax7$^{Low}$ state (Mourikis et al., 2012b; Rocheteau et al., 2012) (Figures 1F and S1E). Taken together, these data demonstrate that RBPJ and NICD signaling regulates the expression of *Odz4*, and by consequence miR-708, in satellite cells *in vivo* by direct binding on distal transcriptional enhancers.

### miR-708 Retains Stemness and Self-Renewal Capacities of Satellite Cells *Ex Vivo*

To assess whether the sustained expression of miR-708 affects satellite cell behavior, we transfected freshly isolated satellite cells with a synthetic miR-708 molecule (Mimic-708; Figures S1F and S1G for validation, specificity) and scored for proliferation with 5-ethynyl-2 -deoxyuridine (EdU$^{+}$) and differentiation (Myogenin$^{+}$). Interestingly, miR-708 overexpression resulted in a delay in cell-cycle entry (24 hr) and proliferative capacity (48 hr) (Figure 1G), and a decrease in the number of MYOG$^{+}$ cells compared to control at 72 hr and 4 days (Figure 1H). Taken together, these results show that miR-708 significantly impedes satellite cell proliferation and differentiation, properties reminiscent of activation of Notch signaling.

In a complementary loss-of-function assay, we depleted miR-708 using short-interfering RNA (AntimiR-708, Figure S1H) in an *ex vivo* system where resident satellite cells on isolated myofibers exit quiescence, enter the myogenic program, and form clusters composed of proliferating (PAX7$^{+}$/MYOD$^{+}$/MYOG$^{-}$), differentiated (PAX7$^{-}$MYOG$^{+}$) and self-renewed (PAX7$^{+}$/MYOD$^{-}$/MYOG$^{-}$) cells (Zammit et al., 2004). Targeting specifically miR-708-5p increased significantly the number of differentiated cells per fiber and reduced the number of proliferating/self-renewing cells (Figure 1I).

A concern with experiments involving miR-708 manipulations is the putative effect on *Odz4* expression, as germline deletion of this gene results in reduced numbers of myofibers and satellite cells (Ishii et al., 2015). However, no miR-708 binding sites were noted in the 3 UTR of *Odz4*, indicating that it is not a miR-708 target. Furthermore, *Odz4* levels were not altered following miR-708 overexpression (Figure S1I). Finally, the induction of miR-708 in *Odz4*-deficient primary satellite cells (Figure S1J) rescued their precocious differentiation phenotype (Figure 1J). Thus, we conclude that, in this context, the anti-myogenic effect of miR-708 was not due to *Odz4* function.

### Antagonism of miR-708 *In Vivo* Induces Spontaneous Exit from Quiescence and Premature Differentiation of Satellite Cells

To investigate the functional role of miR-708 *in vivo*, we synthesized a miR-708 antagonist (AntagomiR-708) with an antisense sequence to mature miR-708-5p, as well as control Scramble. Importantly, real-time qPCR analysis on different cell populations extracted from skeletal muscles, namely, endothelial cells, fibro-adipogenic progenitors, and resident and infiltrating macrophages revealed that only satellite cells expressed miR-708 (data not shown). We then labeled the majority of satellite cells with a tamoxifen-inducible membrane-GFP using *Tg:Pax7-CreERT2; R26*$^{mTmG}$ lineage-traced mice (CT2, CreERT2; ~95% recombination efficiency, Figure S2A). Surprisingly, 10 days after injection (Figure 2A), isolated GFP$^{+}$ cells from resting muscle showed a significant reduction in miR-708 and miR-489 levels, whereas miR-92 expression (activation enriched miRNA, Figure 1A) was strongly upregulated (Figure 2B). In addition, a significant decrease in *Pax7* expression was noted, whereas expression of the activation (*Myod*) and differentiation (*Myogenin*) genes were strongly upregulated following AntagomiR-708 treatment (Figure 2C). Accordingly, *in vivo* immunostaining showed that 18% of mGFP$^{+}$ cells lost PAX7 expression in mice that received AntagomiR-708 during this period (Figure 2D).

(I) miR-708 knockdown using AntimiR-708 transfection of single EDL myofibers from *Tg:Pax7-nGFP* mice cultured for 72 hr and immunostained for GFP and Myogenin. Quantification of PAX7$^{+}$/MYOG$^{-}$ (21% versus 5%), PAX7$^{-}$/MYOG$^{-}$ (36% versus 15%), and PAX7$^{-}$/MYOG$^{+}$ (43% versus 79%) for Scramble and AntimiR-708 populations respectively; 4 mice/condition, n = 25 fibers, is shown.

(J) Satellite cells isolated by FACS from control and *Odz4*-null mice, treated with Mimic or Control for 72 hr and stained for Myogenin. Quantification of Myogenin$^{+}$ cells; n = 3 mice/condition, ≥250 cells, is shown.

Error bars, mean ± SD; two-sided unpaired t test; p value: two-sided paired t test. Scale bars: 50 μm. See also Figure S1.

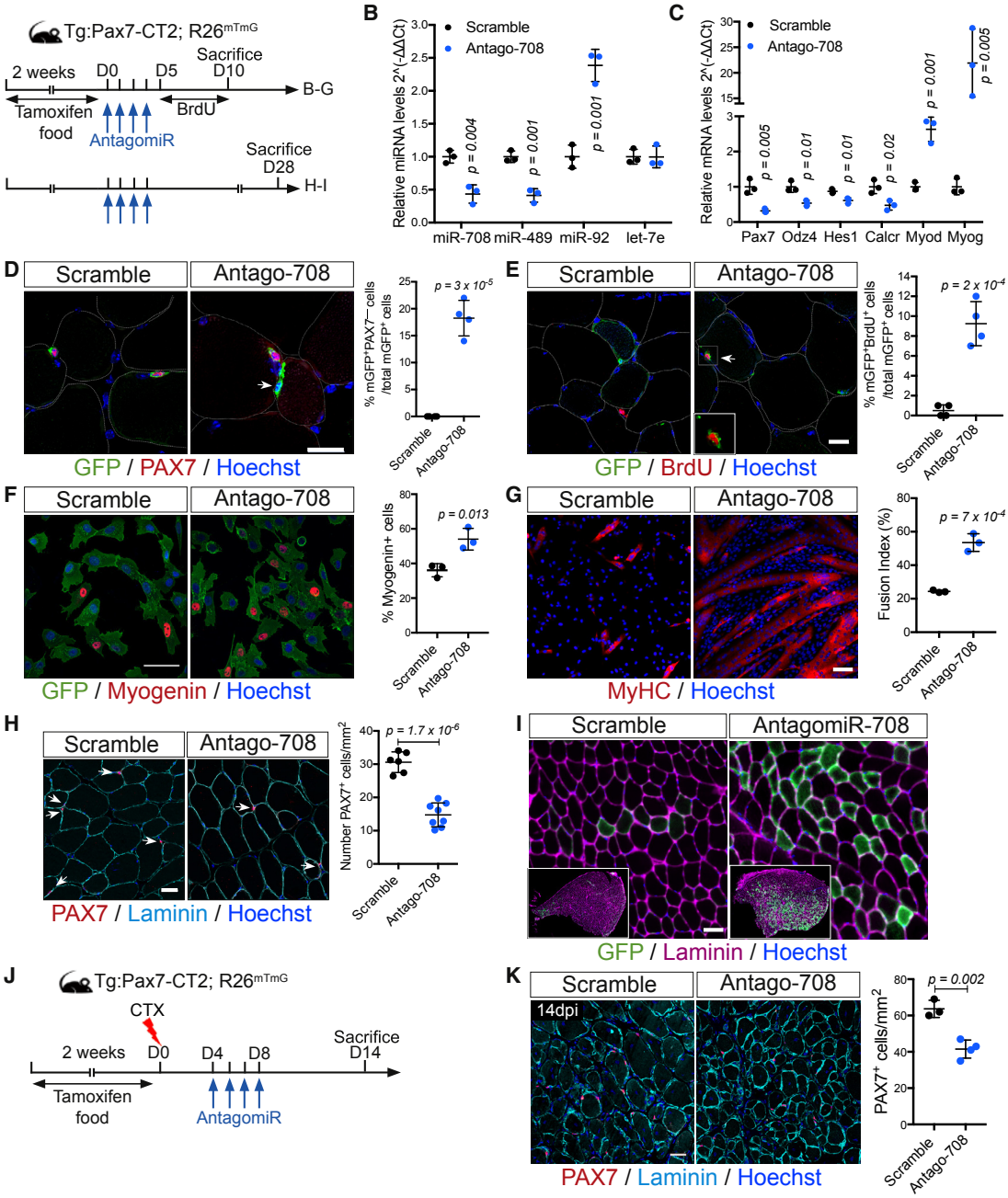


**Figure 2. miR-708 Maintains the Satellite Cell Quiescent State**

(A) Experimental scheme of tamoxifen, AntagomiR, and BrdU administration to *Tg:Pax7-CT2; R26$^{mTmG}$* mice. AntagomiR-708 and Scramble control were injected every day in the tail vein for 4 days after the end of tamoxifen treatment (D0), and mice were analyzed 10 days (B–G) and 28 days (H and I) post-treatment.

(B) miRNA expression in control (Scramble) and miR-708 knockdown (AntagomiR-708) cells isolated by FACS 10 days post-treatment.

(C) mRNA expression in control and AntagomiR-708 cells isolated by FACS 10 days post-treatment.

(D) Representative images of satellite cells on *Tibilias anterior* muscle section from Scramble and AntagomiR-708-treated mice stained for membrane-GFP and PAX7. Quantification of mGFP$^+$/PAX7$^-$ cells (arrow) relative to total mGFP$^+$ cells; n = 4 mice/treatment, is shown.

(E) Membrane-GFP$^+$ satellite cells on TA muscle section from Scramble and AntagomiR-708-treated mouse stained for BrdU. Quantification of mGFP$^+$/BrdU$^+$ cells relative to total mGFP$^+$ cells is shown. Asterisk shows mGFP$^-$/BrdU$^+$ cell; arrows indicate mGFP$^+$/BrdU$^+$ cell; n = 4 mice/treatment.

(F) Myogenin and GFP immunostainings of satellite cells cultured for 72 hr and quantification; n = 3 mice/treatment; ≥150 cells.

(G) Myosin heavy chain (MyHC) staining of satellite cells from Scramble and AntagomiR-708-treated mice isolated by FACS, cultured for 5 days, and quantification of fusion index (nuclei in MyHC$^+$ myotubes with ≥2 nuclei/total number of nuclei); n = 3 mice/treatment, ≥500 nuclei, 2 wells/condition.

(H) Laminin and PAX7 immunostaining on quiescent TA muscle section from Scramble and AntagomiR-treated mice (10 days post-administration) and quantification of PAX7$^+$ cells/mm$^2$; n = 6 Scramble and n = 8 AntagomiR-treated mice.

*legend continued on next page)*

We previously showed that compromised Notch signaling *in vivo* induces satellite cells to differentiate spontaneously without entering S-phase (Mourikis et al., 2012b). However, satellite cells lacking miR-708 incorporated bromodeoxyuridine (BrdU) following activation (Figure 2E), indicating that miR-708 knockdown induces their entry into S-phase prior to differentiation. In addition, satellite cells isolated from AntagomiR-708-treated mice exhibited premature expression of Myogenin (Figure 2F) and consequently an increase in myotube formation as indicated by a higher fusion index (Figure 2G). Taken together, these results indicate that reduced miR-708 levels in satellite cells leads to spontaneous exit from quiescence, activation, and premature differentiation.

Interestingly, long-term inhibition of miR-708 (28 days; Figure 2A) showed a 50% reduction in satellite cell numbers *in vivo* (Figures 2H and S2B). Furthermore, immunostaining with cleaved-caspase 3 showed no significant change in the number of apoptotic cells following AntagomiR-708 treatment (Figure S2C). In contrast, numerous $GFP^+$ fibers were observed in resting muscle indicating that $mGFP^+$ satellite cells spontaneously fused with pre-existing myofibers (Figure 2I). Taken together, these results demonstrate that miR-708 is necessary for maintaining satellite cell quiescence *in vivo*. Of note, transcript analysis of this residual population showed normal levels of miR-708 as well as quiescence and differentiation markers (Figure S2D) suggesting that they escaped AntagomiR-708 treatment.

In the context of muscle damage, AntagomiR-708-treated mice displayed a slight delay in regeneration at 14 days post-injury (dpi) as indicated by smaller myofibers (Figure S2E); however, this delay was not prominent by 31 dpi (Figure S2F). In keeping with this finding, $PAX7^+$ cells were observed at this stage, albeit at much reduced numbers, suggesting that they were escapers. Notably, the severe defect in self-renewal of AntagomiR-treated mice following injury and regeneration (Figures 2J, 2K, and S2G) indicates that miR-708 also regulates re-entry into quiescence.

## miR-708 Promotes Satellite Cell Niche Occupancy *In Vivo* and Regulates Their Motility and Migration Capacities

Suppression of miR-708 has been shown to promote invasion and metastasis of numerous cancer cells types by targeting different genes or pathways involved in the regulation of cell migration (Lin et al., 2015; Ryu et al., 2013). During homeostasis, satellite cells are localized between the myofiber membrane and the basal lamina (Sambasivan and Tajbakhsh, 2015). Surprisingly, we observed abnormal localization of $PAX7^+$ cells in the interstitial space in the TA muscle of AntagomiR-708-treated mice (Figure 3A) suggesting that loss of miR-708 perturbed the anchorage of satellite cells and resulted in their release from their niche.

We confirmed this phenotype by overexpressing miR-708 in freshly isolated satellite cells combined with videomicroscopy (Figure 3B). In addition to the decrease in the number of dividing cells (Figure 1G), the migration distance and velocity of myogenic cells treated with miR-708 were strongly diminished (Figures 3C and 3D; see Video S1). Notably, miR-708 also altered the motility of *Odz4*-depleted satellite cells (Figure S3A) underscoring its specific involvement in this process. Taken together, these results show that miR-708 actively inhibits the migration and motility of satellite cells.

Recently, intravital imaging showed that satellite cell properties can be monitored *in vivo* (Webster et al., 2016). To confirm the observed *in vitro* phenotype directly in muscle, we optimized live microscopy on freshly isolated mouse hind limb explants containing the *Extensor digitorium longus* (EDL) muscle from Scramble- or AntagomiR-treated mice using 2-photon microscopy. Intriguingly, over the 10- to 12-hr imaging period, no displacement was detected in control Scramble ($n = 6$ mice, $\geq 250$ cells, Figure 3E). In contrast, miR-708 silencing *in vivo* resulted in 9% of satellite cells spontaneously exiting their niche and migrating an average distance of $8.7 \pm 6.5$ μm with an average velocity of $7.8 \pm 4.4$ nm/min during the assay period (Figures 3E and 3F; Videos S2, S3, S4, and S5). These experiments provide direct evidence for a role of miR-708 as an active repressor of satellite cell migration.

To identify miR-708 putative targets, we combined three target prediction algorithms (see Figure 3G) and identified 24 overlapping genes, among which 3 were highly expressed in activated compared to quiescent satellite cells (Liu et al., 2013): Tensin3 (*Tns3*), Dickkopf3 (*Dkk3*), and Syndecan-1 (*Sdc1*) (Figure S3B). Their relevance as potential targets was tested by transfection of HEK293 cells with a luciferase reporter vector containing the 3 UTR of *Tns3*, *Dkk3*, or *Sdc1* (Table S2). Notably, miR-708 repressed luciferase activity of both *Dkk3* and *Tns3*, but not *Sdc1* (Figure 3H). Interestingly, only *Tns3* inhibition (Figure S3C) phenocopied the overexpression of miR-708 and significantly decreased cell migration (Figure 3I), whereas *Dkk3* knockdown showed no overt cell motility phenotype (data not shown).

Mutations in *Tns3* miRNA-binding sites significantly decreased miR-708-mediated repression (Figure 3H), as confirmed by a Target Protector assay combined with videomicroscopy (Figure S3D). In keeping with these observations, overexpression of TNS3 in satellite cells was sufficient to rescue the inhibition of migration mitigated by mir-708 (Figure 3J; Video S6). In summary, these findings demonstrate that miR-708 exerts its repressive activity on cell migration primarily through *Tns3*. Finally, given that siTns3 also phenocopied miR-708 inhibition of differentiation (Figure S3E), we propose that miR-708 downregulation during satellite cell activation releases *Tns3* repression to promote satellite cell migration and lineage progression.

(I) Immunostaining for Laminin and GFP on sections from TA muscles of mice 28 days post-Scramble and AntagomiR-708 treatment; inset shows whole TA section; n = 4 mice/treatment.

(J) Schemes of *Tg:Pax7-CT2; R26$^{mTmG}$* mice fed with tamoxifen for 2 weeks, injured with Cardiotoxin (CTX) at D0 followed by daily AntagomiR-708, or Scramble injections for 4 days. Muscles were collected 14 days post-injury.

(K) Laminin and PAX7 immunostaining on injured TA muscle section from Scramble and AntagomiR-treated mice (14 days post-injury) and quantification of $PAX7^+$ cells/$mm^2$; n=3 Scramble and n= 4 AntagomiR treated mice.

Error bars, mean ± SD; two-sided unpaired t test. Scale bar: 25 μm in (D) and (F), 50 μm in (E), (G), (H), and (K), 100 and 300 μm in inset in (I), and 10 μm in inset (E). See also Figure S2.

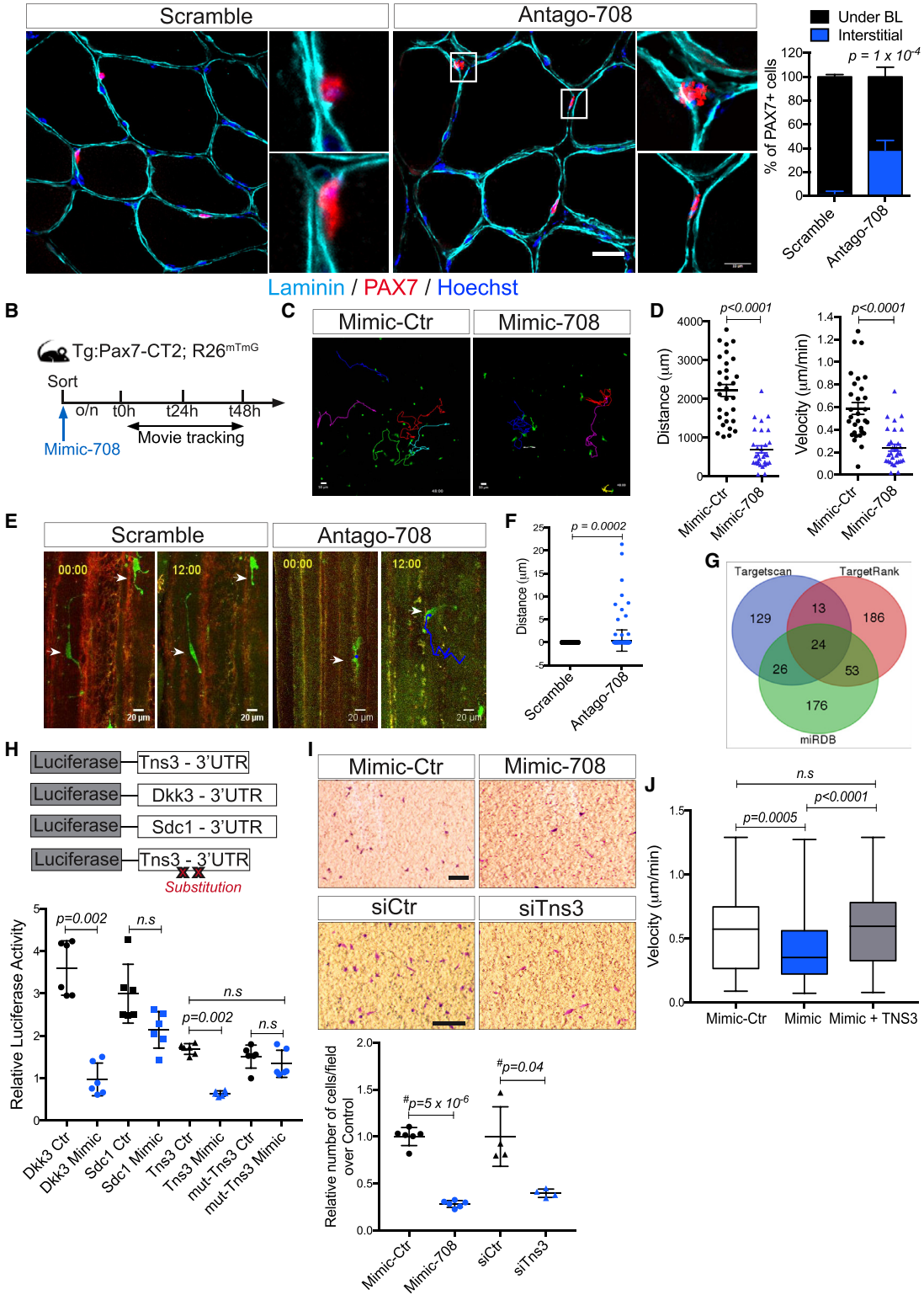


**Figure 3. miR-708 Regulates Myogenic Cell Migration and Motility**

(A) Immunostaining for Laminin and PAX7 on sections from resting TA muscles 10 days post Scramble and AntagomiR-708 treatment and quantification of PAX7$^+$ cells in interstitial space (2% for Scramble versus 38% for AntagomiR-708); n = 4 mice; 2 sections/TA. BL, basal lamina.

(B) Scheme of miR-708 overexpression on membrane-GFP$^+$ satellite cells isolated from *Tg:Pax7-CT2; R26$^{mTmG}$* mice treated 2 weeks with tamoxifen.

*legend continued on next page)*

### Inhibition of Focal Adhesion Kinase Represses Migration and G1-S Transition

Tns3 is a member of focal adhesion (FA)-associated proteins that are important regulators of cell adhesion and migration (Blangy, 2017). Moreover, the Tensin SH2 domain forms a complex with the tyrosine phosphorylated protein FAK allowing its phosphorylation and activation (Qian et al., 2009) (Figure 4A). Notably, miR-708 overexpression in myogenic cells showed a reduction in TNS3 protein levels (Figures 4B and S4A for antibody validation), whereas FAK phosphorylation (p-FAK) levels decreased (Figure 4B). The presence of miR-708 did not affect the ratio of ERK/p-ERK suggesting that p-FAK was inhibited at the local level, rather than by interference of upstream effectors of the migration pathway (Figures 4B and S4B). As observed with miR-708 gain of function, specific inhibition of *Tns3* resulted in downregulation of p-FAK (Figure 4C). In contrast, the absence of miR-708 in primary satellite cells (AntagomiR) resulted in increased levels of TNS3 and p-FAK (Figures 4D and S4C). This decrease in p-FAK was verified by immunostaining satellite cells transfected with either Mimic-708 or siTns3 (Figures 4E and 4E ). Notably, temporal *in vivo* activation showed a rapid increase in *Tns3* expression within 3 hr following injury (Figure S4D) and appearance of TNS3 preceded that of MYOD and cell-cycle entry (Figure S4E) indicating that release of cell migration is an early event during satellite cell activation.

We note that miR-708 overexpression resulted in a delay in cell proliferation of cultured satellite cells (Figure 1G); however, analysis of miR-708 putative targets did not identify cell-cycle regulators. Thus, we propose that the inhibition of migration indirectly inhibits cell-cycle progression. To uncouple proliferation and migration properties, we induced miR-708 in cycling satellite cells isolated from Fucci-Green mice (Fluorescence ubiquitination-based cell cycle indicator), which allows temporal patterns of cell-cycle dynamics using Azami green to label S-G2-M phases (Sakaue-Sawano et al., 2008), combined with live videomicroscopy. Intriguingly, total duration of cell cycle was extended by 25% following miR-708 overexpression (Figure 4F; Video S7), and this was due to a significant extension of G1 (Figures 4G and 4H). These findings indicate that miR-708 exerts cell cycle regulation by modulating the G1 phase of the cell cycle.

## DISCUSSION

A major question in stem cell biology is how cells enter and exit their niche, and how this interaction is stabilized to maintain the stem cell pool for extended periods. Active cell migration is a key property of satellite cells (Siegel et al., 2009), and studies have shown that stimulation of migration improves myogenic cell dispersal following transplantation, thereby resulting in enhanced engraftment efficiency (Bentzinger et al., 2014). Interestingly, reduced levels of Fibronectin and β1-integrin during aging results in loss of satellite cells from their niche (Lukjanenko et al., 2016) thereby underscoring the notion that multiple pathways converge to maintain the stem cell pool. However, it remains unclear how intrinsic regulators modulate the transition into and out of cellular quiescence and how cell division and migration are orchestrated with the anchoring of stem cells in their niche.

In this study, we identified miR-708 as a quiescence-specific mirtron in the *Odz4* gene, where this miRNA acts as a downstream target of Notch signaling to maintain satellite cells within their quiescent niche. Although the mechanism of action of *Odz4* has not been determined in satellite cells, it is intriguing that miR-708 is harbored within this gene, and under the regulation of Notch. Although examples of mirtrons performing regulatory functions have been reported for skeletal and cardiac muscle-specific genes (Cheung et al., 2012; van Rooij et al., 2009), here we provide the first example of such a mirtron that is under the regulation of Notch signaling, and a rare example of a miRNA that controls the maintenance of an adult stem cell population.

*In silico* analysis of miR-708 potential target genes identified *Tns3* that responded in functional assays to this miRNA and phenocopied the functional readouts of miR-708. The role of this Tensin isoform on cell migration is context dependent, and it can act to promote or inhibit cell mobility depending on the presence of co-factors (Qian et al., 2009). However, our findings lead us to propose that TNS3 is maintained at low levels by the action of miR-708 in the anchored quiescent satellite cells via the inhibition of FAK. Upon activation, Notch signaling and hence miR-708 are downregulated, allowing *Tns3* to accumulate and participate in the migration of the activated cells.

(C) Maximum projection of 48-hr time-lapse experiment of $mGFP^+$ cells overexpressing miR-708 (Mimic-708) and Control. Colored line depicts trajectory of a cell for every condition. See Video S1.

(D) Distance and velocity of miR-708-overexpressing cells (Mimic-708) and control were scored for 48 hr; n = 2 mice, n = 30 cells.

(E) Maximum projection of EDL muscle from Scramble or AntagomiR-708-treated mice imaged on an explant at 0 and 12 hr (n = 6 mice/treatment). Arrows point to tracked cells. See Videos S2, S3, S4, and S5.

(F) Migration distance of *in vivo* AntagomiR or Scramble-treated satellite cells on an explant imaged for 12 hr (0 cells displace in Scramble versus 13 cells in AntagomiR); n = 6 mice/treatment; n = 250 cells tracked.

(G) Venn Diagram displaying putative targets of miR-708 as predicted by TargetScan, TargetRank, and MiRDB.

(H) Schemes of *Tns3* (*Tensin-3*), *Dkk3* (*Dickkopf-3*), and *Sdc1* (*Syndecan-1*) constructs and mutated *Tns3* 3′ UTR with relative luciferase activity associated with each in presence (Mimic-708) or absence (Mimic-Ctr) of miR-708. Note the analysis using full 3′ UTR length of *Sdc1* and *Dkk3* and truncated *Tns3* 3′ UTR; n = 6 independent experiments, 2 wells/condition.

(I) Migration properties assessed by transwell assay of miR-708-overexpressing (Mimic-708) or upon Tns3 knockdown (siTns3) compared to control: Mimic-Ctr and siCtr, respectively. Quantification of number of migrating satellite cells through pores of the membrane upon treatment; n = 4 mice, 2 fields counted/membrane, is shown.

(J) Velocity delayed in presence of miR-708 is rescued by overexpression of TNS3. See Video S6.

Error bars, mean ± SD; two-sided unpaired t test (A), Fisher (F), Mann-Whitney test (H and J), two-sided paired t test (I). Scale bar: 50 μm in (A)–(C), 20 μm in (E), and 10 μm in inset in (A) and (I). See also Figure S3.

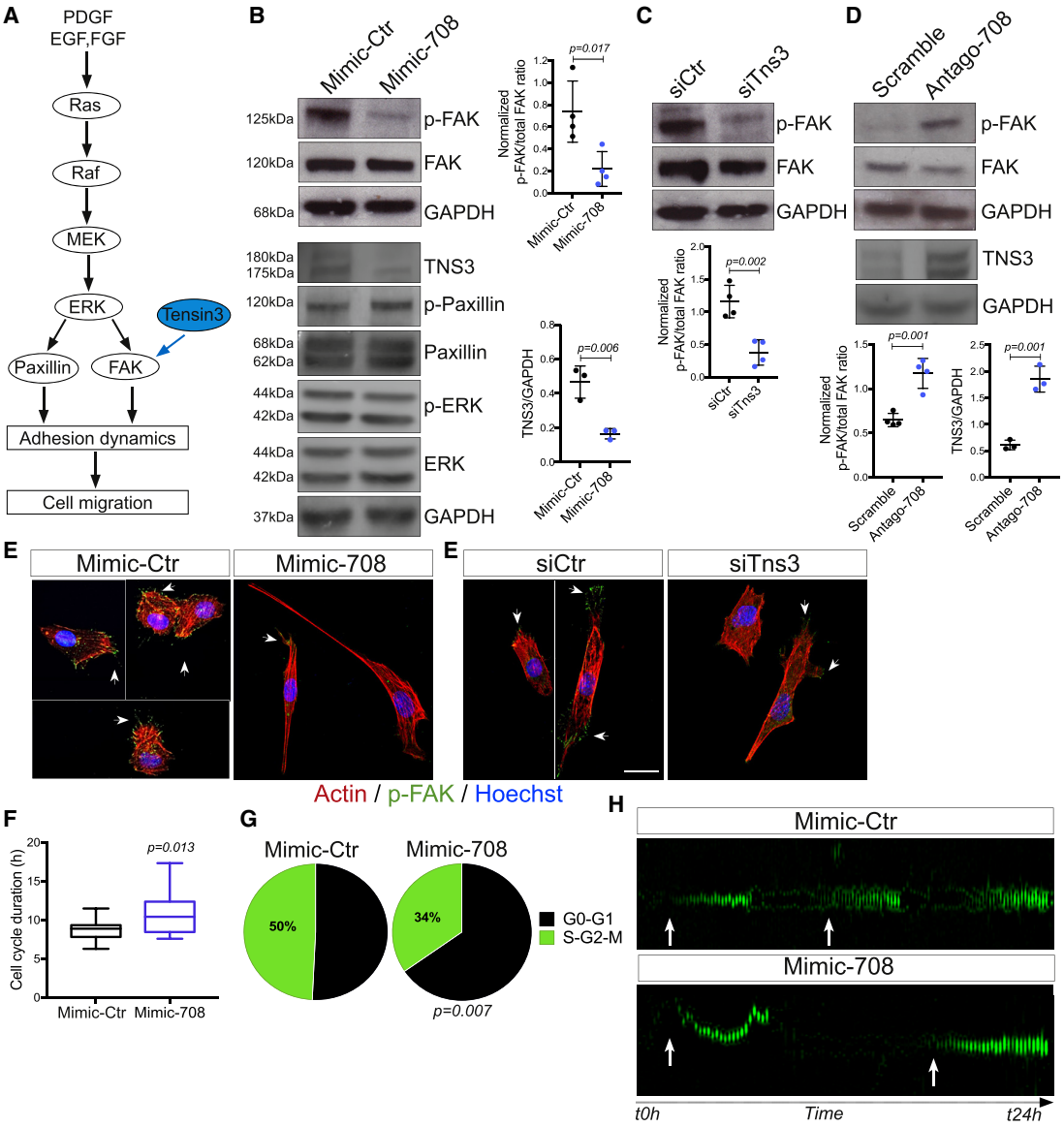


**Figure 4. Tensin3 Inhibition Reduces FAK Activation and Phenocopies miR-708 Overexpression**

(A) Signaling pathway for cell migration mediated by ERK. Growth factors (PDGF, EGF, and FGF) trigger downstream signaling Ras-Raf-MEK that further activate ERK. Activated ERK regulates FA dynamics by phosphorylation of FAK and Paxillin. Tensin3 can interact with FAK (Chen and Lo, 2003).

(B) Western blot showing protein levels and phosphorylation state of FAK, TNS3, Paxillin, and ERK after miR-708 overexpression (Mimic-708) and Control (Ctr) in C2C12 myoblasts; n = 4 independent experiments.

(C) Protein levels and phosphorylation of FAK upon *Tns3* knockdown (siTns3) in C2C12 cells; n = 4 independent experiments.

(D) TNS3 and p-FAK protein levels in freshly isolated satellite cells from Scramble and AntagomiR-treated mice.

All western blots were normalized to GAPDH levels; n = 3–4 mice/condition.

(E and E ) Actin staining with Phalloidin and immunostaining of p-FAK on satellite cells isolated from *Tg:Pax7-nGFP* mouse and transfected with Mimic-708 (E) or siTns3 (E ). Arrowheads show p-FAK positive signal. Two fields from the same culture dish are shown, separated by line; n = 4 mice/condition.

(F) Cell-cycle duration (hours) of satellite cells isolated from Fucci-green mouse treated with Mimic-708 (10 hr avg.) or control (7.5 hr avg.) and tracked for one division.

(G) Cell-cycle repartition of Fucci-green satellite cell following control and miR-708 overexpression (Mimic-708). Cells were tracked for one cell cycle.

(H) Time series of a Fucci-green satellite cell transfected with Mimic-708 or control with corresponding kymograph. Distance between two arrows represents one cell cycle; n = 3 mice, 15 cells tracked/condition. See Video S7.

Error bars, mean ± SD, two-sided unpaired t test (B–D), Mann-Whitney test (F and G). Scale bar: 25 μm. See also Figure S4.

Interestingly, FAK has been shown to regulate cell-cycle progression by modulating the G1/S transition (Zhao et al., 1998). Therefore, we propose that indirect inhibition of FAK by miR-708 could be responsible of this extension of the G1/S transition. Our observations are concordant with a previous study showing that FAK signaling regulates cell-cycle progression via the

activation of *cyclin D1 Ccnd1)* transcription through EtsB binding site of the *Ccnd1* promoter (Zhao et al., 2001).

In summary, we provide the first evidence that inhibition of the migration capacity of a stem cell is essential for maintaining the quiescent cell within its niche. We uncover a regulatory axis where Notch induces transcription of the quiescence specific mirtron miR-708 that represses Tensin3, a major component of the FA complex, to inhibit FAK activation, which in turn stabilizes satellite cells within their niche. For quiescent stem cells to enter or exit their niche, they need to coordinate their final mitosis as well as cell migration. Given that satellite cells are rarely found to be subjacent, our results lead us to speculate that satellite cells continue to migrate after their last mitosis, and then migration is suppressed through miR-708 as cells are then anchored in their niche. These findings suggest that mitosis and migration might be negotiated sequentially in other quiescence stem cell populations.

## STAR METHODS

Detailed methods are provided in the online version of this paper and include the following:

- KEY RESOURCES TABLE
- CONTACT FOR REAGENT AND RESOURCE SHARING
- EXPERIMENTAL MODEL AND SUBJECT DETAILS
  - Animals
- METHOD DETAILS
  - Muscle injury, tamoxifen and BrdU administration
  - Satellite cell dissociation and fluorescence activated cell sorting (FACS)
  - RNA extraction and quantitative PCR (RT-qPCR)
  - Satellite cell culture and transfection
  - Single myofiber isolation and antimir transfection
  - Immunostaining of cells, myofibers and sections
  - AntagomiR synthesis and administration
  - Transwell Assay
  - Construction of luciferase reporters, mutagenesis and luciferase assays
  - Target Protector assay
  - Western Blot
  - *Ex vivo* videomicroscopy
  - Live videomicroscopy of muscle explants
- QUANTIFICATION AND STATISTICAL ANALYSIS
  - Statistical analysis
- DATA AND SOFTWARE AVAILABILITY

### SUPPLEMENTAL INFORMATION

Supplemental Information includes four figures, two tables, and seven videos and can be found with this article online at https://doi.org/10.1016/j.stem.2018.09.017.

### ACKNOWLEDGMENTS

We would like to thank C. Akazawa, N. Suzuki, and K. Ishii (Tokyo Medical and Dental University, Tokyo, Japan) for kindly providing *Odz4* KO muscle samples, O. Burri for helping with movie processing, and A. Seitz for use of BIOP facilities. We thank A. Blangy for TNS3 plasmids and antibodies, Y. Wang for kindly performing some of the tail vein injections, and the Center for Translational Science, Institut Pasteur. S.T. acknowledges support from the Institut Pasteur, Agence Nationale de la Recherche (Laboratoire d'Excellence Revive, ANR-10-LABX-73), Association Française contre les Myopathies, CNRS, and the European Research Council (Advanced Research Grant 332893). M.B.B. was supported by a doctoral school fellowship and Fondation pour la Recherche Médicale.

### AUTHOR CONTRIBUTIONS

S.T. and M.B.B. proposed the concept and designed the experiments. M.B.B. performed and analyzed most of the experiments. D.C. performed the RNA sequencing. D.D.G. initiated the western blot experiments. J.F. processed and analyzed the *in vitro* videomicroscopy. P.M. generated the enhancer plasmids. B.E. optimized section immunostainings and designed the cloning strategies. K.S. performed and analyzed the *ex vivo* explant imaging. M.B.B. and S.T. wrote the paper. All authors read and agreed on the manuscript.

### DECLARATION OF INTERESTS

The authors declare no competing interests.

Received: December 25, 2017
Revised: July 18, 2018
Accepted: September 27, 2018
Published: November 8, 2018

### REFERENCES

Baghdadi, M.B., and Tajbakhsh, S. (2018). Regulation and phylogeny of skeletal muscle regeneration. Dev. Biol. *433*, 200–209.

Baghdadi, M.B., Castel, D., Machado, L., Fukada, S.I., Birk, D.E., Relaix, F., Tajbakhsh, S., and Mourikis, P. (2018). Reciprocal signalling by Notch-Collagen V-CALCR retains muscle stem cells in their niche. Nature *557*, 714–718.

Bentzinger, C.F., von Maltzahn, J., Dumont, N.A., Stark, D.A., Wang, Y.X., Nhan, K., Frenette, J., Cornelison, D.D., and Rudnicki, M.A. (2014). Wnt7a stimulates myogenic stem cell motility and engraftment resulting in improved muscle strength. J. Cell Biol. *205*, 97–111.

Bjornson, C.R., Cheung, T.H., Liu, L., Tripathi, P.V., Steeper, K.M., and Rando, T.A. (2012). Notch signaling is necessary to maintain quiescence in adult muscle stem cells. Stem Cells *30*, 232–242.

Blangy, A. (2017). Tensins are versatile regulators of Rho GTPase signalling and cell adhesion. Biol. Cell *109*, 115–126.

Bröhl, D., Vasyutina, E., Czajkowski, M.T., Griger, J., Rassek, C., Rahn, H.P., Purfurst, B., Wende, H., and Birchmeier, C. (2012). Colonization of the satellite cell niche by skeletal muscle progenitor cells depends on Notch signals. Dev. Cell *23*, 469–481.

Castel, D., Mourikis, P., Bartels, S.J., Brinkman, A.B., Tajbakhsh, S., and Stunnenberg, H.G. (2013). Dynamic binding of RBPJ is determined by Notch signaling status. Genes Dev. *27*, 1059–1071.

Castel, D., Baghdadi, M.B., Mella, S., Gayraud-Morel, B., Marty, V., Cavaillé, J., Antoniewski, C., and Tajbakhsh, S. (2018). Small-RNA sequencing identifies dynamic microRNA deregulation during skeletal muscle lineage progression. Sci. Rep. *8*, 4208.

Chen, H., and Lo, S.H. (2003). Regulation of tensin-promoted cell migration by its focal adhesion binding and Src homology domain 2. Biochem. J. *370*, 1039–1045.

Cheung, T.H., Quach, N.L., Charville, G.W., Liu, L., Park, L., Edalati, A., Yoo, B., Hoang, P., and Rando, T.A. (2012). Maintenance of muscle stem-cell quiescence by microRNA-489. Nature *482*, 524–528.

Haldar, M., Karan, G., Tvrdik, P., and Capecchi, M.R. (2008). Two cell lineages, myf5 and myf5-independent, participate in mouse skeletal myogenesis. Dev. Cell *14*, 437–445.

Han, H., Tanigaki, K., Yamamoto, N., Kuroda, K., Yoshimoto, M., Nakahata, T., Ikuta, K., and Honjo, T. (2002). Inducible gene knockout of transcription factor recombination signal binding protein-J reveals its essential role in T versus B lineage decision. Int. Immunol. *14*, 637–645.

Hicks, C., Ladi, E., Lindsell, C., Hsieh, J.J., Hayward, S.D., Collazo, A., and Weinmaster, G. (2002). A secreted Delta1-Fc fusion protein functions both as an activator and inhibitor of Notch1 signaling. J. Neurosci. Res. *68*, 655–667.

Ishii, K., Suzuki, N., Mabuchi, Y., Ito, N., Kikura, N., Fukada, S., Okano, H., Takeda, S., and Akazawa, C. (2015). Muscle satellite cell protein Teneurin-4 regulates differentiation during muscle regeneration. Stem Cells *33*, 3017–3027.

Kirby, T.J., Chaillou, T., and McCarthy, J.J. (2015). The role of microRNAs in skeletal muscle health and disease. Front Biosci (Landmark Ed) *20*, 37–77.

Krutzfeldt, J., Rajewsky, N., Braich, R., Rajeev, K.G., Tuschl, T., Manoharan, M., and Stoffel, M. (2005). Silencing of microRNAs in vivo with "antagomirs". Nature *438*, 685–689.

Lin, K.T., Yeh, Y.M., Chuang, C.M., Yang, S.Y., Chang, J.W., Sun, S.P., Wang, Y.S., Chao, K.C., and Wang, L.H. (2015). Glucocorticoids mediate induction of microRNA-708 to suppress ovarian cancer metastasis through targeting Rap1B. Nat. Commun. *6*, 5917.

Liu, L., Cheung, T.H., Charville, G.W., Hurgo, B.M., Leavitt, T., Shih, J., Brunet, A., and Rando, T.A. (2013). Chromatin modifications as determinants of muscle stem cell quiescence and chronological aging. Cell Rep. *4*, 189–204.

Livak, K.J., and Schmittgen, T.D. (2001). Analysis of relative gene expression data using real-time quantitative PCR and the 2(-Delta Delta C(T)) method. Methods *25*, 402–408.

Lukjanenko, L., Jung, M.J., Hegde, N., Perruisseau-Carrier, C., Migliavacca, E., Rozo, M., Karaz, S., Jacot, G., Schmidt, M., Li, L., et al. (2016). Loss of fibronectin from the aged stem cell niche affects the regenerative capacity of skeletal muscle in mice. Nat. Med. *22*, 897–905.

Mourikis, P., Gopalakrishnan, S., Sambasivan, R., and Tajbakhsh, S. (2012a). Cell-autonomous Notch activity maintains the temporal specification potential of skeletal muscle stem cells. Development *139*, 4536–4548.

Mourikis, P., Sambasivan, R., Castel, D., Rocheteau, P., Bizzarro, V., and Tajbakhsh, S. (2012b). A critical requirement for notch signaling in maintenance of the quiescent skeletal muscle stem cell state. Stem Cells *30*, 243–252.

Murtaugh, L.C., Stanger, B.Z., Kwan, K.M., and Melton, D.A. (2003). Notch signaling controls multiple steps of pancreatic differentiation. Proc. Natl. Acad. Sci. USA *100*, 14920–14925.

Muzumdar, M.D., Tasic, B., Miyamichi, K., Li, L., and Luo, L. (2007). A global double-fluorescent Cre reporter mouse. Genesis *45*, 593–605.

Qian, X., Li, G., Vass, W.C., Papageorge, A., Walker, R.C., Asnaghi, L., Steinbach, P.J., Tosato, G., Hunter, K., and Lowy, D.R. (2009). The Tensin-3 protein, including its SH2 domain, is phosphorylated by Src and contributes to tumorigenesis and metastasis. Cancer Cell *16*, 246–258.

Rocheteau, P., Gayraud-Morel, B., Siegl-Cachedenier, I., Blasco, M.A., and Tajbakhsh, S. (2012). A subpopulation of adult skeletal muscle stem cells retains all template DNA strands after cell division. Cell *148*, 112–125.

Ruby, J.G., Jan, C.H., and Bartel, D.P. (2007). Intronic microRNA precursors that bypass Drosha processing. Nature *448*, 83–86.

Ryu, S., McDonnell, K., Choi, H., Gao, D., Hahn, M., Joshi, N., Park, S.M., Catena, R., Do, Y., Brazin, J., et al. (2013). Suppression of miRNA-708 by polycomb group promotes metastases by calcium-induced cell migration. Cancer Cell *23*, 63–76.

Sakaue-Sawano, A., Kurokawa, H., Morimura, T., Hanyu, A., Hama, H., Osawa, H., Kashiwagi, S., Fukami, K., Miyata, T., Miyoshi, H., et al. (2008). Visualizing spatiotemporal dynamics of multicellular cell-cycle progression. Cell *132*, 487–498.

Sambasivan, R., and Tajbakhsh, S. (2015). Adult skeletal muscle stem cells. Results Probl. Cell Differ. *56*, 191–213.

Sambasivan, R., Gayraud-Morel, B., Dumas, G., Cimper, C., Paisant, S., Kelly, R.G., and Tajbakhsh, S. (2009). Distinct regulatory cascades govern extraocular and pharyngeal arch muscle progenitor cell fates. Dev. Cell *16*, 810–821.

Seale, P., Sabourin, L.A., Girgis-Gabardo, A., Mansouri, A., Gruss, P., and Rudnicki, M.A. (2000). Pax7 is required for the specification of myogenic satellite cells. Cell *102*, 777–786.

Shinin, V., Gayraud-Morel, B., Gomès, D., and Tajbakhsh, S. (2006). Asymmetric division and cosegregation of template DNA strands in adult muscle satellite cells. Nat. Cell Biol. *8*, 677–687.

Siegel, A.L., Atchison, K., Fisher, K.E., Davis, G.E., and Cornelison, D.D. (2009). 3D timelapse analysis of muscle satellite cell motility. Stem Cells *27*, 2527–2538.

Tinevez, J.Y., Perry, N., Schindelin, J., Hoopes, G.M., Reynolds, G.D., Laplantine, E., Bednarek, S.Y., Shorte, S.L., and Eliceiri, K.W. (2017). TrackMate: An open and extensible platform for single-particle tracking. Methods *115*, 80–90.

van Rooij, E., Quiat, D., Johnson, B.A., Sutherland, L.B., Qi, X., Richardson, J.A., Kelm, R.J., Jr., and Olson, E.N. (2009). A family of microRNAs encoded by myosin genes governs myosin expression and muscle performance. Dev. Cell *17*, 662–673.

Webster, M.T., Manor, U., Lippincott-Schwartz, J., and Fan, C.M. (2016). Intravital imaging reveals ghost fibers as architectural units guiding myogenic progenitors during regeneration. Cell Stem Cell *18*, 243–252.

Zammit, P.S., Golding, J.P., Nagata, Y., Hudon, V., Partridge, T.A., and Beauchamp, J.R. (2004). Muscle satellite cells adopt divergent fates: A mechanism for self-renewal? J. Cell Biol. *166*, 347–357.

Zhao, J.H., Reiske, H., and Guan, J.L. (1998). Regulation of the cell cycle by focal adhesion kinase. J. Cell Biol. *143*, 1997–2008.

Zhao, J., Pestell, R., and Guan, J.L. (2001). Transcriptional activation of cyclin D1 promoter by FAK contributes to cell cycle progression. Mol. Biol. Cell *12*, 4066–4077.

# STAR METHODS

## KEY RESOURCES TABLE

| REAGENT or RESOURCE | SOURCE | IDENTIFIER |
|---|---|---|
| Antibodies | | |
| α7-integrin-APC (1 :1000) | Ablab | clone R2F2 |
| CD34-e450 (1 :50) | eBioscience | clone RAM34 |
| Sca1-Pe-Cy7 (1 :400) | eBioscience | clone D7 |
| CD45-Pe-Cy7 (1 :100) | eBioscience | clone 30-F11 |
| CD31-PE (1 :50) | BD | clone MEC13.3 |
| Chick GFP (1 :2000) | Abcam | 13970 |
| Mouse PAX7 (1 :40) | DHSB | AB_528428 |
| Mouse Myosin Heavy Chain (1 :40) | DHSB | MF20 |
| Mouse Myogenin (1 :40) | DHSB | clone F5D |
| Mouse MYOD (1 :100) | DAKO | M3512 |
| Mouse anti-BrdU (1 :100) | BD | 347580 |
| Rabbit Laminin (1 :500) | Sigma | L9393 |
| Rhodamine Phalloidin (Actin) (1 :1000) | Invitrogen | R415 |
| Tensin 3 (M-300) (1 :100) | Santa Cruz | sc134909 |
| Phospho-FAK (Tyr397) (1:200 for IF and 1:1000 for WB) | Cell Signaling | 3238 |
| FAK (1 :1000) | BD Biosciences | 610087 |
| Phospho-Paxillin (Tyr118) (1 :1000) | Cell Signaling | 2541 |
| Paxillin (1 :1000) | BD | Clone 165 |
| Phospho-p44/42 MAPK (Erk1/2) (1 :1000) | Cell Signaling | 9101 |
| p44/42 MAPK (Erk1/2) (1 :1000) | Cell Signaling | 4695 |
| Tensin3 (C-terminal) (1 :1000) | Sigma, SAB4200205 | 1088866 |
| GAPDH (1 :4000) | Santa Cruz, sc25778 | FL-335 |
| HRP-conjugated goat anti-rabbit | Pierce | 31460 |
| HRP-conjugated goat anti-mouse | Pierce | 31430 |
| Tamoxifen food pellets | Tamoxifen diet Harlan | TD.55125 |
| Snake venom cardiotoxin | Lotaxan | L8102 |
| DNase | Roche | 11284932001 |
| Collagenase A | Roche | 11088793001 |
| Dispase II | Roche | 04942078001 |
| Ultroser G | Pall Biosepra | 15950-017 |
| Matrigel | Corning | 354248 |
| BrDU | Sigma | B5002 |
| Lipofectamine 2000 | ThermoFicher | 11668 |
| Transwell | Corning | 3428 |
| Crystal Violet | Sigma | C0775 |
| 4%–12% Bis-Tris Gel NuPAGE | Invitrogen | NP0322 |
| Low melting agarose | Sigma | A9414 |
| Commercial Assays | | |
| EdU Click it | Thermo Fisher | C10640 |
| Target Protecttor | QIAGEN | 219000 |
| Q5® site-directed mutagenesis | NEB | E0554S |
| SuperScriptIII® enzyme | Invitrogen | 18080093 |
| miRCURY LNA® universal RT | Exiqon | 203301 |
| ExiLENT SYBR® green | Exiqon | 339345 |

(*Continued on next page*)

| *ontinued* | | |
|---|---|---|
| REAGENT or RESOURCE | SOURCE | IDENTIFIER |
| Dual Glo® luciferase assay | Promega | 2920 |
| Pierce ECL2 western blotting | Thermo Scientific | 80196 |
| Deposited Data | | |
| small RNA-seq | Castel et al., 2018 | E-MTAB-5955 |
| Notch ChIP-seq | Castel et al., 2013 | GEO: GSE37184 |
| Satellite cells microarray | Liu et al., 2013 | GEO: GSE52192 |
| Videos S1, S2, S3, S4, S5, S6, and S7 | Mendeley | https://dx.doi.org/10.17632/xhrjsbwg92.1 |
| Experimental Models: Cell Lines | | |
| C2C12 | The Weizmann Institute of Science (Israel) | N/A |
| HEK293T | Institut Pasteur | N/A |
| Experimental Models: Organisms/Strains | | |
| *Myf5$^{Cre}$* | The corresponding lab | (Haldar et al., 2008) |
| *R26$^{stop\text{-}NICD\text{-}nGFP}$* | The corresponding lab | (Murtaugh et al., 2003) |
| *R26$^{mTmG}$* | The corresponding lab | (Muzumdar et al., 2007) |
| *Rbpj$^{flox/flox}$* | The corresponding lab | (Han et al., 2002) |
| Fucci-Green | The corresponding lab | (Sakaue-Sawano et al., 2008) |
| *Tg:Pax7-CreERT2* | Generated in Tajbakhsh lab | (Mourikis et al., 2012b) |
| *Tg:Pax7-nGFP* | Generated in Tajbakhsh lab | (Sambasivan et al., 2009) |
| *Odz4* KO | The corresponding lab | (Ishii et al., 2015). |
| Oligonucleotides | | |
| RT-qPCR primers | | Table S1 |
| Recombinant DNA | | |
| 3 UTR sequences | | Table S2 |
| pGL3-Control vector | Promega | E1741 |
| Software and Algorithms | | |
| Imagej | Open source | https://imagej.nih.gov/ij/download.html |
| Zen | Open source | https://www.zeiss.fr/microscopie/produits/microscope-software/zen-lite.html |
| Prism | | https://www.graphpad.com |

## CONTACT FOR REAGENT AND RESOURCE SHARING

Further information and requests for resources and reagents should be directed to and will be fulfilled by the Lead Contact, Shahragim Tajbakhsh (shahragim.tajbakhsh@pasteur.fr).

## EXPERIMENTAL MODEL AND SUBJECT DETAILS

### Animals

Animals housing, husbandry and handling were performed in the animal facility of Institut Pasteur in accordance with the national and European community guidelines. The health and immune status of all mice used were normal, and they were not involved in any previous procedures. Food and water were administered *ad libitum*. For Notch *in vivo* gain-of-function, *Myf5$^{Cre}$* mice (Haldar et al., 2008) were crossed with *R26$^{stop\text{-}NICD\text{-}nGFP}$* (Murtaugh et al., 2003), and fetuses were recovered 14.5 days post-fertilization. For Notch *in vivo* knock-down, *Tg:Pax7-CreERT2* (Mourikis et al., 2012b) was crossed with *Rbpj$^{flox/flox}$* (Han et al., 2002) and the lineage tracing mouse line *R26$^{mTmG}$* (Muzumdar et al., 2007). The *Tg:Pax7-nGFP* mouse line was generated in the Tajbakhsh lab (Sambasivan et al., 2009) with a BAC containing approximately 200 kbp of mouse genomic DNA including the locus encoding *Pax7* and sequences both upstream (~55 kbp with respect to Pax7 initiator ATG) and downstream (~60 kbp from terminator codon). The targeting vector was designed to introduce nGFP (nuclear GFP) into the first exon of Pax7 gene (mutated initiator ATG and deleted bases 58-94 of exon 1). *Odz4* KO mice were kindly provided by Drs. Chihiro Akazawa and Nobuharu Suzuki (Ishii et al., 2015) and Fucci-Green mice (Sakaue-Sawano et al., 2008) by Dr. Atsushi Miyawaki. All experiments were performed indistinguishably with mice of both sexes from 6 to 8 weeks of age. All protocols were approved by ethics committee at Institut Pasteur and the French Ministry.

## METHOD DETAILS

### Muscle injury, tamoxifen and BrdU administration

For muscle injury, mice were anesthetized with 0.5% Imalgene/2% Rompun and the TA muscle was injected with 50 μL of Cardiotoxin (10mM; Latoxan, L8102). *Tg:Pax7-CreERT2; Rbpj$^{flox}$; R26$^{mTmG}$* and *Tg:Pax7-CreERT2; R26$^{mTmG}$* were fed with tamoxifen containing diet for two weeks (Envigo, TD55125). Five days prior sacrifice mice were given the thymidine analog 5-Bromo-2 -deoxyuridine (BrdU, 0.5mg/ml, Sigma, B5002) in the drinking water supplemented with sucrose (25mg/ml). Comparisons were done between age-matched littermates using 8-12-week old mice.

### Satellite cell dissociation and fluorescence activated cell sorting FACS)

Adult and fetal limb muscles were dissected, minced and incubated with a mix of Dispase II (Roche, 04942078001) 3U/ml, Collagenase A (Roche, 11088793001) 100ug/ml and DNase I (Roche, 11284932001) 10mg/ml in Hank's Balanced Salt Solution (HBSS, GIBCO) supplemented with 1% Penicillin-Streptomycin (PS; GIBCO) at 37°C at 60rpm in a shaking water bath for 2h. The muscle suspension was successively filtered through 100μm and 70μm cell strainers (Milteny, 130-098-463 and 130-098-462) and then spun at 50 g for 10min at 4°C to remove large tissue fragments. The supernatant was collected and washed twice by centrifugation at 600 g for 15min. Prior to FACS, the final pellet was resuspended in cold Dulbecco's Modified Eagle Medium (DMEM, GIBCO) supplemented with 1%PS and 2% Fetal Bovine Serum (FBS, GIBCO) and the cell suspension was filtered through a 40μm strainer (BD, 352340).

For satellite cell isolation from Fucci-green and *Odz4* KO mice, cells were stained with α7-integrin-APC (Ablab, clone R2F2, 1/1000), CD34-e450 (eBioscience, clone RAM34, 1/50), Sca1-Pe-Cy7 (eBioscience, clone D7, 1/400), CD45-Pe-Cy7 (eBioscience, clone 30-F11, 1/100) and CD31-PE (BD, clone MEC13.3, 1/50). Satellite cells were sorted with an Aria III (BD Biosciences).

### RNA extraction and quantitative PCR RT-qPCR)

Micro-RNAs from cells or tissue were purified using (QIAGEN miRNAeasy® Micro Kit) and reverse transcribed in cDNA using miRCURY LNA® universal RT kit (Exiqon, 203301). Expression of mature miRNAs was determined using ExiLENT SYBR® green master mix (Exiqon) and miRNA LNA™ PCR primers (Exiqon; hsa-miR-708-5p, 204490; mmu-miR-489-3p, 205036; hsa-let-7e-5p, 205711; mmu-miR-92-5p, 205947). Two snoRNA; RNU5G (Exiqon, 308014) and SNORD65 (Exiqon, 308016) were used for normalization.

Total mRNAs were isolated using (QIAGEN RNAeasy® Micro Kit) and reverse transcribed using SuperScriptIII® enzyme (Invitrogen, 18080093). The eventual remaining RNAs were degraded by incubation 20 min at 37°C with RNase H endonuclease (Roche, 10786357001). Expression of mature mRNAs was assessed with SYBR green master mix (Roche, 04913914001) and analysis were performed using the $2^{-CT}$ method (Livak and Schmittgen, 2001). All RT-qPCR samples were normalized with *Tbp* and *Rpl13*. Specific forward and reverse primers used for RT-qPCR are listed in Table S1.

### Satellite cell culture and transfection

Satellite cells were isolated by FACS, and total muscle preparations were seeded at $3x10^3$ cells/cm$^2$ on Matrigel® (Corning, 354248) coated dishes for 30 min at 37°C. Cells were cultured in a growth medium (GM) containing DMEM/F12 (50:50; GIBCO), 1% PS, 20% FBS, 2% Ultroser (Pall, 15950-017) and incubated at 37°C, 3% $O_2$, 5% $CO_2$ for the indicated time. Half of the medium was changed every 3 days. To assess proliferation, cells were pulsed with the thymidine analog 5-ethynyl-2 -deoxyuridine (EdU), $1x10^{-6}$ M, 2h prior to fixation (ThermoFisher Click-iT Plus EdU kit, C10640).

Freshly isolated satellite cells from *Tg:Pax7-nGFP* were transfected in suspension with miRIDIAN microRNA mmu-miR-708-5p mimic (AAGGAGCUUACAAUCUAGCUGGG, Dharmacon, C310987) and Scramble Control 1 (UCACAACCUCCUAGAAAGA GUAGA; Dharmacon, CN-001000) at 200nM final concentration using Lipofectamine 2000 (ThermoFisher, 11668) in Opti-MEM (GIBCO). Four hours after transfection, 3 volumes of fresh growth medium were added and cells were cultured for the indicated time. Cells were fixed with 4% paraformaldehyde (PFA) in PBS 10 min at room temperature (RT).

### Single myofiber isolation and antimir transfection

Single myofibers were isolated from *Extensor digitorum longus* (EDL) muscles following the previously described protocol (Shinin et al., 2006). Briefly, EDL muscles were dissected and incubated in 0.1% w/v collagenase (Sigma, C0130)/DMEM for 1h in a 37°C shaking water bath at 40rpm. Following enzymatic digestion, mechanical dissociation was performed to release individual myofibers that were then transferred to serum-coated Petri dishes. Single myofibers were transfected with miRCURY LNA™ mmu-miR-708-5p inhibitor (AAGGAGCUUACAAUCUAGCUGGG, Exiqon, 4101225) or Scramble Control A (Exiqon, 199096) at a final concentration of 250nM, using Lipofectamine 2000 (ThermoFisher, 11668) in Opti-MEM (GIBCO). Four hours after transfection, 6 volumes of fresh satellite cell growth medium was added and fibers were cultured for 72h at 37°C, 3%$O_2$. Fibers were fixed with 4%PFA/PBS 15 min at room temperature.

### Immunostaining of cells, myofibers and sections

Following fixation, cells and myofibers were washed three times with PBS, then permeabilised and blocked at the same time in buffer containing 0.25% Triton X-100 (Sigma), 10% goat serum (GS; GIBCO) for 30min at RT. For BrdU immunostaining, epitopes were

unmasked with DNase I (1000 U/ml, Roche, 04536282001) for 30 min at 37°C. Cells and fibers were then incubated with primary antibodies overnight at 4°C. Samples were washed with 1X PBS three times and incubated with Alexa-conjugated secondary antibodies (Life Technologies, 1/1000) and Hoechst (Life Technologies, 1/10000) for 45 min at RT. EdU staining was chemically revealed using the Click-iT Plus kit according to manufacturer's recommendations (Life Technologies, C10640). For Phalloidin staining, cells were fixed in 3%PFA/2% Sucrose for 15 min at RT, permeabilised with 0.1% Triton for 10 min and incubated with Rhodamine Phalloidin for 30 min at RT.

Isolated *Tibialis anterior* (TA) muscles were frozen in liquid-nitrogen cooled isopentane and sectioned transversely at 8 μm. Sections were post-fixed with 4%PFA overnight at 4°C and washed 3 times with 1X PBS. For antibody staining of transcription factors, antigen retrieval was performed by incubating sections in boiling 10mM Tris-EDTA buffer pH9 in a 2100 Retriver device.

Confocal images were acquired with Zeiss LSM700 microscope and Zen Blue 2.0 software. Quantifications were done on the whole TA muscle section taken from two distally located regions in the muscle for each mouse acquired with Zeiss Axioscan Z1.

### AntagomiR synthesis and administration

AntagomiR and Scramble were designed as described before (Krutzfeldt et al., 2005). PAGE-purified AntagomiR were synthetized with the following modifications (Dharmacon):

AntagomiR-708: 5 mC*mC*mCmAmGmCmUmAmGmAmUmUmGmUmAmAmGmCmU*mC*mU*mU*3 -Chl;
Scramble:
5 mU*mU*mUmCmUmAmAmUmCmAmAmGmGmGmUmCmUmGmUmG*mG*mC*mU*3 -Chl. Where * represents phosphothiotate linkage at given position; m, 2 OMethyl-modified nucleotides; Chl, cholesterol linked through a hydroxyprolinol linkage. AntagomiR molecules were resuspended in saline and injected every day for 4 days into tail veins at a dose of 8 μg/g of mouse.

### Transwell Assay

The bottom part of a transwell membrane with 8 μm pores size (Corning, 3428) was coated with Matrigel 15min at 37°C. FACS isolated satellite cells from *Tg:Pax7-nGFP* mouse were culture as described before for 24h prior to Mimic or siRNA transfection. Twenty-four hours (for Mimic) or 48h (for siRNA) post-transfection, myogenic cells where trypsinized (GIBCO, 25200) 10 min at 37°C. Trypsin was washed away by the addition of DMEM/10% FCS and cells were centrifuged 15min at 600 g. Cell pellets were resuspended in a low serum medium DMEM/2% FCS and seeded on the upper part of the transwell. Cells were allowed to migrate in a vertical direction through the pores of the membrane into the lower compartment, in which higher serum content was present (growth medium). Six hours after seeding, the membrane was fixed 15min with methanol and non-migrated cells remaining on the topside of the filter were removed with a cotton swab. The migrated cells were stained with Crystal Violet 0.5%/ 25% Methanol for 5min (Sigma, C0775) and washed 5 times in 1X PBS.

### Construction of luciferase reporters, mutagenesis and luciferase assays

For the generation of luciferase reporters, candidate enhancers of *Odz4* were amplified by PCR from genomic DNA of C2C12 cells. The enhancers were then cloned into the firefly-luciferase pGL3-Basic vector (Promega, E1751) upstream of a minimal thymidine kinase promoter (minTK) as described previously (Castel et al., 2013). Twenty-four hours after transfection, C2C12 cells were trypsinized and plated on Dll-Fc or control Fc for 24h before luciferase activity measurement. For Dll1-Fc and Fc protein production, conditioned medium was prepared from stable 293T cell lines, transfected with the corresponding plasmid as previously described (Hicks et al., 2002).

The full 3 UTR length of mouse *Dkk3* (2.5kb) and *Sdc1* (1.8kb) (http://genome.ucsc.edu) were amplified by PCR from reverse transcribed cDNA from total RNA extract of E17.5 mouse fetuses (Table S2). Partial *Tns3*-3 UTR (500bp) containing miR-708 potential binding site of interest was obtained from SourceBioscience (EST clone: IMAGp998D088514Q) (Table S2). 3 UTR were cloned in the pGL3-Control vector (Promega, E1741) at the XbaI site downstream of the luciferase gene. Targeted mutagenesis was performed using the Q5® site-directed mutagenesis kit (NEB, E0554S) according to manufacturer's guidelines. HEK293T were co-transfected with the plasmid of interest and Mimic-708 or Scramble negative control and cultured in DMEM/10%FCS, at 37°C, 5% $CO_2$, and 20% $O_2$ for 48h before luciferase assay. In both assays, a Renilla luciferase plasmid (pCMV-Renilla) was also co-transfected as transfection control and empty pGL3 vector was used as a background negative control. Firefly and renilla luciferase activities were detected with Dual Glo® luciferase assay system (Promega, 2920) and the results were expressed as firefly luciferase activity relative to Renilla luciferase activity.

### Target Protector assay

Freshly isolated satellite cells from *Tg:Pax7-nGFP* mice were transfected using miScript Target Protector according to the manufacturer's recommendation (QIAGEN, 219000). Briefly, Script Target Protector (10nM final) and miRNA Mimic (500nM final) were transfected using Lipofectamine 2000 as described above.

### Western Blot

C2C12 cells were transfected with Mimic (final concentration 200nM) or siRNA (siTns3 L063982, siDkk3 L060631, Scramble D0018100205, Dharmacon, final concentration 250nM) as described above and cultured in DMEM/10%FCS, at 37°C, 5% $CO_2$, and 20% $O_2$ for 48h. Primary satellite cells were sorted directly in lysis buffer (150M NaCl, 50mM Tris pH8, 5mM EDTA, 1% NP-40 (Sigma, I8896), 0.5% sodium deoxycholate, 0.1% SDS supplemented with 1X proteases (Sigma, S8820) and phosphatases (Roche, 4906845001) inhibitors) and $5x10^4$ cells were loaded/lane. Total protein extracts were run on a 4%–12% Bis-Tris Gel NuPAGE (Invitrogen, NP0322) and transferred on a PVDF Amersham Hybond-P transfer membrane (Ge Healhcare, RPN303F). The membrane was then blocked with 5% BSA (Sigma, A9418) in Tris-Buffer Saline (TBS) for 1h at RT and probed with specific primary antibodies overnight at 4°C. After three washes in TBS1X-Tween 0.2%, membrane was incubated with HRP-conjugated goat anti-rabbit (1:3000, Pierce, 31460) or anti-mouse (1:10000, Pierce, 31430) IgG secondary antibodies, and revealed by chemiluminescence (Pierce ECL2 western blotting substrate, Thermo Scientific, 80196). All western blots bands were quantified using ImageJ software.

### *Ex vivo* videomicroscopy

Cells were transfected and seeded as indicated above. The plate was then incubated at 37°C, 5% $CO_2$, and 3% $O_2$ (Zeiss, Pecon). A Zeiss Observer.Z1 connected to an LCI PlnN 10 /0.8 W objective and Hamamatsu Orca Flash 4 camera piloted with Zen (Zeiss) was used. Cells were imaged every 13 min for the time indicated. Distance and velocity plots were obtained using the Manual tracking plugin available in Fiji (Figure 3D) or automatic tracking (remaining experiments) provided by TrackMate (Tinevez et al., 2017) after contrast enhancement using a median filter followed by "Detect Edges" functions available in FIJI. Track parameters were kept within the same datasets; track segment splitting was allowed with a maximal distance between time frames of 50 μm. For the kymograph, cells were manually tracked and a fixed ROI of 150px by 150px containing the cell in its center was extracted for each time point. A line encompassing the cell nucleus was drawn and the Dynamic Reslice plugin in Fiji was used to obtain the corresponding kymograph.

### Live videomicroscopy of muscle explants

Live imaging was performed on the *Extensor digitorum longus* (EDL) in an explant culture system. The EDL was kept attached to the bone from tendons on both sides while the remaining leg muscles were carefully removed. The explant was immobilized on a 50mm glass bottom dish (Mattek Co, P50G-0-30-F) coated with 1% low melting agarose (Sigma, A9414) and cultured in satellite cell GM supplemented with 20mM $NaHCO_3$ at 37°C, 5% $CO_2$. Imaging was conducted on a Zeiss LSM7MP microscope with a 2-photon laser (Chameleon Laser from Coherent) at 860nm and a Zeiss Plan-Apochromat 20x/0.8 M27 objective. Z stacks of 160-200 um were acquired with a step of 2.5 μm. GFP and tdTomato were simultaneously detected using 2 NDD detectors with the following bandpass filters: BP 575-610 and BP 640-710. Movies had a duration of 10-12h with a 30min interval. A maximum intensity projection (MIP) of all optical sections was done using Zen Blue software from Carl Zeiss. The "Correct 3D drift" plugin available in Fiji was then applied to the MIP and afterward the "Manual Tracking" plugin in Fiji was employed to obtain the relevant data (velocities and distance).

## QUANTIFICATION AND STATISTICAL ANALYSIS

### Statistical analysis

No statistical methods were used to predetermine sample size. The investigators were not blinded to allocation during experiments and outcome assessment. No animal has been excluded from analysis and no randomization method has been applied in this study. For comparison between two groups, two- tailed paired, unpaired Student's t tests or Mann-Whitney test were performed to calculate P values and to determine statistically significant differences. The number of independent experimental replications (n value 3: mice, fetuses, experiments, wells or counted cells/muscles), the definition of center, variation (mean ± SD) and statistical test (P value) are reported in each corresponding figure legend. Fisher test was used to compare phenotypic variations in Figure 3F. All statistical analyses were performed with GraphPad Prism software.

## DATA AND SOFTWARE AVAILABILITY

The small RNA-seq are available in the ArrayExpress database at EMBL-EBI under accession number E-MTAB-5955 (Castel et al., 2018). Notch ChIP-seq data are available under the accession number GEO Accession number GEO: GSE37184 (Castel et al., 2013). Microarray analysis on freshly isolated and activated satellite cells data are available under the GEO accession number GEO: GSE52192 (Liu et al., 2013). Supplementary videos are available at https://dx.doi.org/10.17632/xhrjsbwg92.1.